Mode-Locked Laser Diodes and Their Monolithic Integration

John H. Marsh, *Fellow, IEEE*, and Lianping Hou, *Member, IEEE*

(Invited Paper)

***Abstract*—We describe mode locked laser diodes (MLLDs) operating from 40 GHz to >1 THz. Below 40 GHz, operation at the fundamental cavity frequency is appropriate, but at higher frequencies harmonic mode-locking (HML) is used. To increase output power and control nonlinear behavior, the gain needs to be modified, and an AlGaInAs/InP structure with a three-quantum-well active layer and passive far-field reduction layer is presented. In 40-GHz all-active MLLDs, this structure offers improvements in internal loss, slope efficiency, mode locking (ML) range, RF linewidth, timing jitter, far field pattern, and coupling efficiency to a single-mode fiber. By creating a transparent passive waveguide in part of the cavity, a 490-fs pulse width was achieved, the shortest reported from any quantum well MLLD. Several approaches are described for HML: colliding pulse ML operating up to 240 GHz, coupled cavity ML up to 160 GHz, and sampled Bragg grating constructions up to 1.28 THz. This latter approach offers stable HML over a wide range of bias conditions. Finally, we report a synchronized multicolor ML laser array, containing four 40-GHz lasers with designated wavelength registration for optical code division multiple access or optical time division multiple access applications.**

***Index Terms*—Semiconductor lasers, semiconductor laser arrays, quantum well lasers, distributed Bragg reflector lasers, laser modes.**

I. Introduction

GENERATION of ultrafast and ultrashort optical pulses is of great interest for future large capacity optical communication networks, including high-bit-rate optical time-division-multiplexing systems and ultrafast data processing. Mode-locked laser diodes (MLLDs) are very attractive and promising candidates for this purpose because they have excellent pulse characteristics compared to other optical pulse sources and can produce short pulse widths ranging from picoseconds to sub-picoseconds with small frequency chirp. They can provide these pulses at high repetition frequencies, exceeding tens and even hundreds of gigahertz [1]–[3]. In addition, the lasers are compact, robust, cheap to manufacture, and can be integrated with other semiconductor elements, such as semiconductor optical amplifiers (SOAs).

In passive mode-locking (ML), the longitudinal modes of a laser are locked in phase, phase locking being achieved at the fundamental round trip frequency of the cavity by placing a saturable absorber (SA) adjacent to one facet. The laser then produces a series of pulses whose period is that of the cavity round trip time. By virtue of their short cavity length, MLLDs offer higher ML frequencies than any other type of laser. However, practical constraints on the cavity length limit the fundamental ML repetition frequency to around 80 to 170 GHz for a MLLD with a typical cavity length between 0.5 and 1 mm [4].

A robust solution for generating higher frequency pulse streams is to utilize harmonic ML (HML) techniques. An HML laser produces an optical pulse train at a harmonic of the fundamental round-trip frequency of the device. This can be achieved by methods including sub-harmonic optical injection [5], colliding pulse ML (CPM) [6]–[9], compound-cavity ML (CCM) [10]–[12], methods based on the selectivity of harmonic numbers related to the spectral-filtering properties of conventional distributed Bragg reflector (DBR) lasers [10], and techniques we proposed based on sampled grating DBRs (SGDBRs) [13], [14]. We have recently taken this concept further and demonstrated the use of novel SGDBRs in which a π-phase shifted grating is placed in the section where there would be no grating in a conventional SGDBR (C-SGDBR). We denote such gratings as π-phase shifted SGDBR (PPS-SGDBR) [15]. Compared with the C-SGDBR, the PPS-SGDBR has a significantly larger effective coupling coefficient which results in a clearer and sharper reflection comb while retaining the precise wavelength spacing that determines the ML frequency [15].

In this paper we will discuss the relative advantages of the different device constructions. In Section II, the approach to integration and the epitaxial structures are described. We then describe the operation of a simple 40 GHz MML operating at the fundamental cavity round trip frequency in Section III. Colliding Pulse Mode-Locking (CPM) and Coupled Cavity Mode-Locking (CCM) are discussed in Sections IV and V respectively. To reach very high frequencies (>200 GHz) the finite length of the SAs in CPM lasers become a limiting factor, while CCM lasers require high precision cleaving. Devices based on SGDBRs, which allow the highest frequencies to be achieved, are reported in Section VI. Finally, a monolithic multi-color MML array is reported in Section VII.

Manuscript received January 30, 2017; revised March 17, 2017; accepted April 2, 2017. This work was supported in part by the U.K. Engineering and Physical Sciences Research Council under Grant EP/E065112/1 and by the National Science Foundation of China under Grant 61320106013. *(Corresponding author: John H. Marsh).*

The authors are with the School of Engineering, University of Glasgow, Glasgow, G12 8QQ U.K (e-mail: john.marsh@glasgow.ac.uk; lianping.hou@glasgow.ac.uk).

Color versions of one or more of the figures in this paper are available online at http://ieeexplore.ieee.org

Digital Object Identifier 10.1109/JSTQE.2017.2693020

II. Fabrication and Material Structure

In the work reported here, we have used the AlGaInAs/InP material system, as previous research indicated that it has better intrinsic characteristics compared to the more conventional InGaAsP/InP system [16]. One of the challenges in using this material system is oxidation of the Al-containing layers, which becomes a critical concern when the active waveguide core is exposed during etch and regrowth stages of fabrication. Accordingly, we have used a very flexible re-growth free approach for device fabrication, based on ridge waveguides to provide lateral confinement, and quantum well intermixing (QWI) to modify the bandgap along a device [17], [18]. Using this approach, we can integrate MLLDs monolithically with other components, such as semiconductor optical amplifiers (SOAs) to increase the output average power [19]–[20], electro-absorption modulators and photodiodes, and DBRs to provide wavelength control and wavelength tuning and to determine the ML repetition frequency [21], [22]. Here we use a side-wall or surface etched grating DBR which can be simultaneously fabricated along with the ridge waveguide, eliminating the need for overgrowth [21].

The epitaxial structure needs to be customized depending on the characteristics of the particular laser. Partly because of the limited gain of semiconductor structures operating at 1.5 μm, it is often desirable to use long laser cavities and to use HML for high frequency ML. In such cases, epitaxial designs with low internal loss and high saturation energy (E_{sat}) in the gain section are desirable [23]. This can be achieved by reducing the optical overlap with the QW and reducing the number of QWs. We have used either a conventional design of wafer containing 5 quantum wells (5-QW) or a novel design with 3 quantum wells (3-QW).

Semiconductor lasers for high power operation are designed with a long cavity to dissipate heat, and a reduced optical overlap with the QWs to control nonlinear effects. Using such approaches, a world-leading power of 29 W at roll-over was reported for a 100 μm stripe laser at 940 nm [24]. We have applied a similar methodology to increase the average output power of CPM lasers without increasing the duration of the pulses. The epitaxial design which was developed used a smaller number of QWs [2], [25] resulting in reduced internal losses ($\alpha_{\rm i}$) and a high saturation energy ($E_{sat} = h\nu A/(\Gamma dg/dN)$, where $h\nu$ is the photon energy, *A* is the mode area, *dg/dN* is the differential gain, and Γ is the optical confinement factor). Fewer QWs result in a reduction of α_i, Γ and *dg/dN*, and thus provide a higher E_{sat}, which is essential to deliver stable ML operation [25]. In order to further increase the average output power whilst enlarging the range of bias parameters to enable ML without increasing the pulse pedestal, the modal area *A* should be increased, which will naturally decrease the value of $\alpha_{\rm i}$ and Γ, and increase the value of E_{sat}. This also has the benefit of reducing the angular spread of the far-field pattern (FFP), enabling a simplified, and high-yield optical alignment when used in practical applications. Further advantages of a longer laser cavity include a decrease of the spectral linewidth of each longitudinal mode [26], and enhancement of the four wave mixing process and associated phase correlation between modes through a reduced optical mode spacing [27].

The 5-QW epitaxial structure was grown on a sulfur-doped InP substrate via metal-organic vapor phase epitaxy (MOVPE) using a single growth step [16]. The 1.55 μm AlGaInAs multi-quantum-well (MQW) layer consisted of five (6 nm thick) compressively strained (1.2%) wells and six (10 nm thick) tensile strained (-0.3%) barriers. The MQWs were located in the center of the graded-index, separate-confinement heterostructure (GRINSCH) layer (60 nm on each side). The GRINSCH layer terminated at a 60 nm thick $Al_{0.423}Ga_{0.047}In_{0.53}As$ waveguide layer. The active region was followed by a 50 nm *p*-InP, 20-nm-thick *p*-type InGaAsP quaternary wet etch stop layer with a bandgap wavelength of 1.1 μm (1.1Q), and a 1.6 μm thick *p*-type InP cladding layer with a graded doping profile. The top contact layer was a heavily p^+-doped, 200 nm thick InGaAs layer.

The 3-QW structure had a similar waveguide core but with the number of QWs reduced to 3 and incorporated a passive 160 nm thick far-field reduction layer 1.1Q ($In_{0.85}Ga_{0.15}As_{0.33}P$) (FRL) separated from the waveguide core by a 0.75-μm-thick *n*-InP spacer layer [23]. The FRL, which is essentially a much weaker waveguide in terms of a refractive index value when compared to the waveguide core in the active region, was incorporated in the *n*-cladding layer to expand the optical near-field in the vertical direction, towards the *n*-cladding layer side. The repositioning of the mode reduces the modal loss related to free carrier and inter-band absorption in the heavily doped *p*-cladding layer, and suppresses higher order transverse mode lasing [28]. The FRL concept also has the advantage of reducing the divergence angle and low timing jitter, while suppressing higher order transverse mode lasing [25], [28].

III. 40 GHz Mode-Locked Laser Diodes

We will first consider a simple construction designed to operate at the fundamental round trip frequency of the cavity, with a single SA placed adjacent to one of the facets. The performance of 5-QW and 3-QW structures will be compared to highlight the improvement from the latter. The devices have a total length of 1070 μm and consist of a gain section (1040 μm), and a 20 μm long SA (see Fig. 1), designed to give a mode-locked frequency, F_r, of around 40 GHz. Samples were cleaved into individual laser bars with both facets left uncoated and were mounted epilayer-up on a temperature controlled copper heat sink, which was kept constant at 20 °C. Samples were tested under CW conditions.

The left hand side of Fig. 2 shows the characteristics of the 5-QW devices. Fig. 2(a) shows the typical light-current (*L-I*) characteristics and threshold current change for the 5-QW structure with different reverse bias voltages applied to the short SA. The threshold current with an unbiased absorber section at 20 °C is 24 mA. Increasing the reverse voltage on the SA raises the threshold current and reduces the slope efficiency, as a result of an increase in inter-band and exciton absorption. The slope efficiency is about 14.0% at a reverse bias voltage of 0 V. The

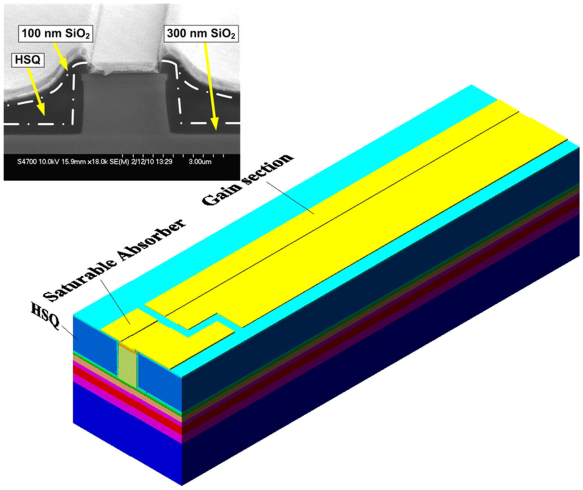

Fig. 1. Schematic of 40 GHz AlGaInAs/InP mode-locked laser and scanning electron microscope (SEM) picture of the cross section of the device (top inset). Hydrogen Silsequioxane (HSQ) was used to planarize the ridge waveguide of the device.

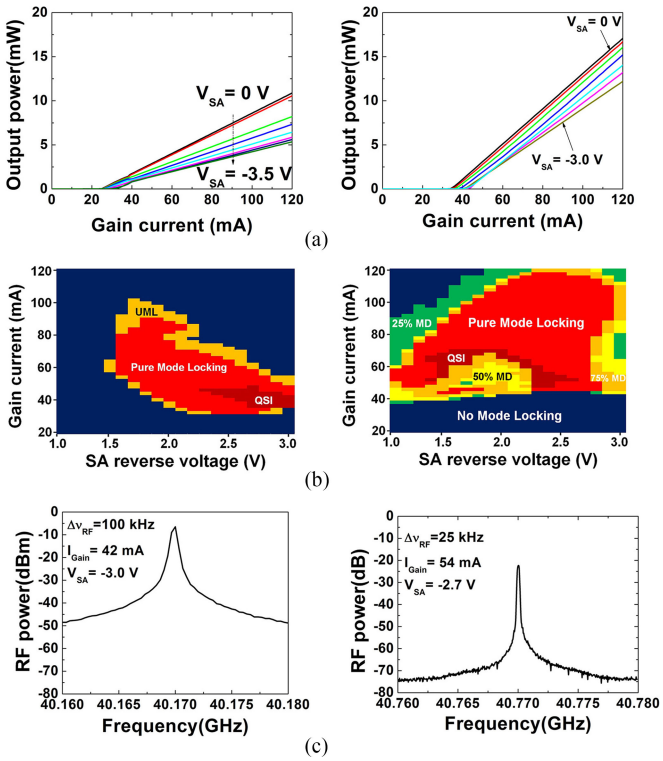

Fig. 2. Comparison of 40 GHz MLLDs based on 5-QW (left side) and 3-QW (right side): (a) Typical *L-I* characteristics for varied applied reverse voltage on the SA section, V_{SA}, (b) experimental map of ML regime of laser operation vs I_{Gain} and V_{SA}, and (c) narrowest measured RF spectrum with $I_{Gain} = 42\,\text{mA}, V_{SA} = -3.0\,\text{V}$ and $I_{Gain} = 54\,\text{mA}, V_{SA} = -2.7\,\text{V}$ for 5-QW and 3-QW respectively.

estimated internal loss is as low as $\sim$15 cm^{-1}, calculated by the Hakki-Paoli method.

Passive ML of the device was obtained by forward biasing the gain section (I_{Gain}) and reverse biasing the absorber section (V_{SA}). A range of behaviors of the pulse train can be observed, depending on the bias conditions. These include pure ML with

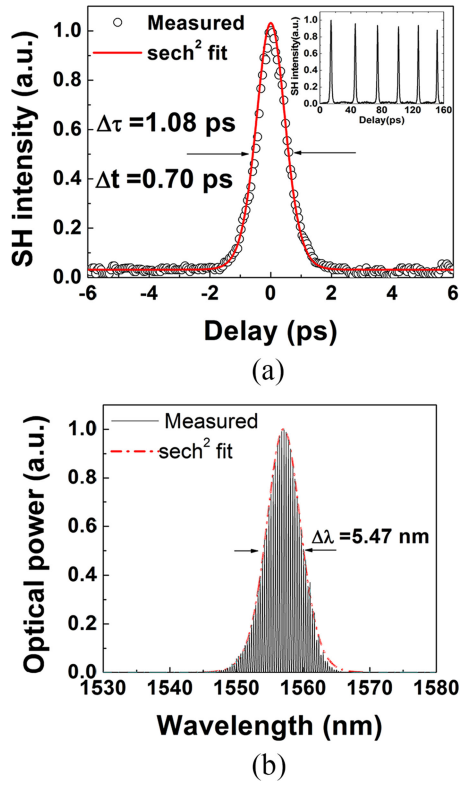

Fig. 3. (a) Measured isolated pulse fitting by sech^2 shape and autocorrelation pulse trains (inset) and (b) optical spectrum. In both cases $I_{Gain} = 42\,\text{mA}$, $V_{SA} = -3.0\,\text{V}$ for the 5-QW MLLD.

100% modulation, ML accompanied by Q-switching instabilities (QSI), incomplete ML with a shallow modulation depth (MD), and unstable mode-locking (UML).

The ML map is shown in the left hand side of Fig. 2(b). Pure ML is obtained for injection currents, from 36 mA to 90 mA and SA biases from -1.6 to -3.0 V, where the absorber recovery time is suitably fast [29].

We have compared our results with calculations performed with the phenomenological travelling wave model LasTiDom [30], and obtained close agreement. In these calculations, geometrical parameters were taken from experiment, gain model parameters (in the two-parameter logarithmic approximation) from the literature [31], the voltage dependence of the SA recovery time was deduced from [29], and the unsaturated absorption was adjusted to approximately reproduce the measured threshold current variation with voltage seen in Fig. 2(a).

The pulse width was measured using autocorrelation via second-harmonic-generation (SHG). The FWHM values of the autocorrelation traces ranged from 1.08 to 5.04 ps, depending on the values of both V_{SA} and I_{Gain}. We note typical trends, i.e., pulses broaden with increasing I_{Gain} and shorten with increasing V_{SA}. This is due to the stronger self-phase modulation (SPM) accompanying an increased gain saturation with increasing I_{Gain} [32], and exponentially decreasing absorber recovery times with increasing reverse voltage, respectively [29]. The shortest measured autocorrelation width of an isolated pulse was 1.08 ps, which deconvolves to a 0.7 ps pulse duration assuming a sech^2 pulse shape [see Fig. 3(a)]. To the best of our

TABLE I
3-QW COMPARED WITH 5-QW STRUCTURE FOR 40 GHz MLLD

Parameters		3-QW	5-QW
Optical overlap with QWs (Γ) (%)		2.19	5
Internal loss (cm^{-1})		8	15
Slope efficiency for FP laser with 1070 μm cavity length (%)		21	14
Pure ML regime	(V)	$-1 > V_{SA} > -2.9$	$-1.6 > V_{SA} > -3.0$
	(mA)	$46 < I_{Gain} < 118$	$36 < I_{Gain} < 90$
Narrowest RF linewidth (kHz)		25	~100
Shortest pulse length (ps)		<1	0.7
RMS timing jitter (from 10 kHz to 100 MHz) (ps)		1.2	4.4
FFP (H × V)		21.8° × 25.6°	34.7° × 35.1°

knowledge, the 700 fs pulse duration is the shortest obtained from conventional two-section passive C-band quantum-well semiconductor MLLs without any applied external pulse compression scheme, even shorter than that of the specially designed InGaAsP/InP counterparts [25]. The >10 ps pulse durations recently reported for λ~1.55 μm InAs/InP quantum dot (QD) two-section MLLs are comparatively long compared with those obtained from quantum well lasers at the same wavelength, as reported here and elsewhere [33], [34]. The 700 fs pulse duration is also comparable to that obtained from the single-section QD [35] or quantum-dash [36] MLLs at a nominal wavelength of 1.55 μm.

The period of the measured emitted pulse train was 24.9 ps [see inset of Fig. 3(a)], corresponding to the obtained RF spectrum signal at 40.17 GHz. RF measurements were carried out using a spectrum analyzer (3 Hz–50 GHz, E4448A from Agilent Technologies). The measured RF spectral line width at half maximum of the RF signal was about 100 kHz (with 100 kHz resolution bandwidth), with the peak value of more than 50 dB over the noise floor [see Fig. 2(c)]. The root mean square (rms) timing jitter of the device was 4.4 ps, calculated from the integration of the single-side-band (SSB) phase noise spectrum over the offset frequency range of 10 kHz to 100 MHz. Compared to the typical jitter value of 12.5 ps observed in two-section quantum well passively MLLs [37], our device demonstrated an approximate three-fold improvement.

The optical spectrum (measured with 0.06 nm resolution bandwidth) was centered at 1557 nm with a 3 dB bandwidth of 5.47 nm [see Fig. 3(b)]. The time-bandwidth product of the pulse is equal to 0.48, which is somewhat larger than the transform limit (≈ 0.315) of a pulse with a $sech^2$ pulse shape. This is likely to be due to SPM in the gain section [32].

We now consider the characteristics of lasers fabricated using the 3-QW epitaxial structure. Characteristics for the 3-QW structure are shown on the right hand side of Fig. 2. The slope efficiency and output power for the same drive current are significantly higher [see Fig. 2(a)]. These improvements reflect a reduced internal loss of ~8 cm^{-1}. The ML maps are compared in Fig. 2(b), where it can be seen the area of pure ML is substantially larger for the 3-QW laser. The RF linewidth is reduced from 100 kHz to 25 kHz FWHM [see Fig. 2(c)].

A comparison between the 3-QW and 5-QW results is summarized in Table I. For the reasons outlined above, the 3-QW laser has much better performance in terms of all of the following: internal loss reduced from 15 to 8 cm^{-1}; slope efficiency from a single facet increased from 14% to 21%; wider pure ML regime in terms of V_{SA} and I_{Gain}; narrowest RF linewidth reduced from 100 to 25 kHz; RMS timing jitter reduced from 4.4 to 1.2 ps (integrated from 10 kHz to 100 MHz); and the FFP reduced by nearly 10° in both the horizontal and vertical directions. The reduction in FFP allowed the butt-coupling efficiency to single mode fiber to be increased from 10% to 20%.

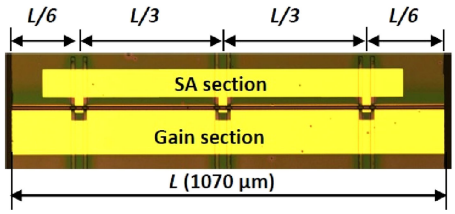

Fig. 4. Optical microscope picture of the 240 GHz CPM device (top view), indicating its dimensions and the positions of the three SA sections.

The pulse length can be further reduced by making part of the cavity a transparent passive waveguide [38]. In this case the device had a total length of 1155 μm with a gain section of 700 μm, a 25 μm long SA, and an extended passive section of 450 μm. The passive waveguide was fabricated by QWI. Waveguide losses of 4.5 cm^{-1} (passive) and 8 cm^{-1} (active) were measured over the wavelength range from 1500 to 1580 nm using the Fabry–Pérot and Hakki-Paoli techniques respectively. Without any external pulse compression, nearly transform-limited Lorentzian pulses were generated at a ~38 GHz repetition frequency with a pulse duration of 490 fs, which is the shortest pulse duration from any directly electrically pumped QW MLLD. The ML range was very large and the pulse width very stable over a broad range of driving conditions [38].

IV. COLLIDING PULSE MODE LOCKING (CPM)

Higher pulse-repetition frequencies can be achieved with a longer cavity using HML techniques, and one way to realize this is to use the colliding-pulse ML (CPM) configuration [6]–[9]. In a CPM laser, one or more SAs are placed at strategic points in the cavity, rather than adjacent to one of the facets as in fundamental frequency ML. Several pulses circulate in the cavity and interfere (collide) in the SAs. For example, a single SA placed in the centre of a cavity will favour ML at the 2nd harmonic. The monolithic CPM laser is a compact light source which is thermally and mechanically very stable, and can be made using relatively simple fabrication processes, while having less stringent cleaving tolerances compared with the compound-cavity design discussed in Section V.

We have used the CCM technique and a 3-QW wafer structure to fabricate 240 GHz MLLDs [39]. The fabricated device optical microscope pictures and dimensions and the positions of the three SA sections are shown in Fig. 4.

Passive ML of the device was achieved by forward biasing the gain sections and reverse biasing the SA sections. The purest 6^{th} harmonic (i.e., ML frequency (F_r) of ~240 GHz with ~100% pulse modulation with a negligible pedestal), was obtained

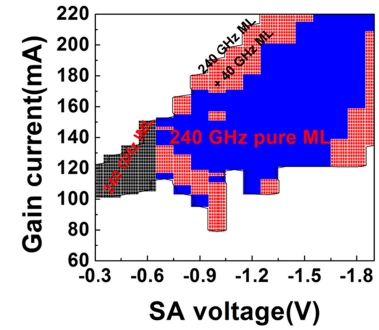

(a)

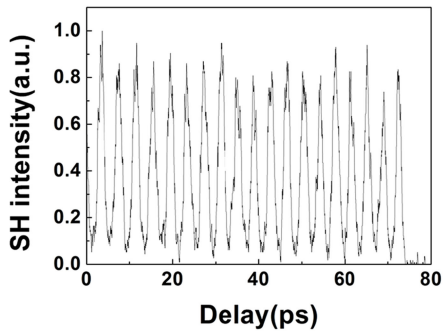

(b)

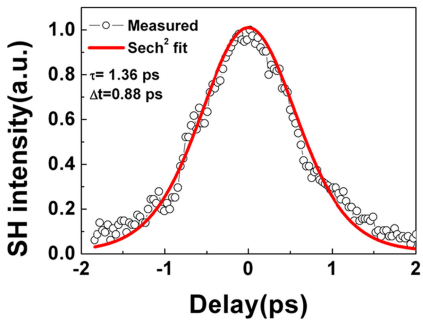

(c)

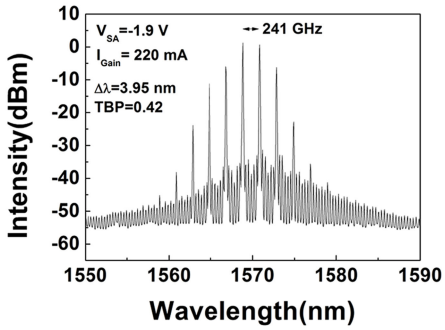

(d)

Fig. 5. (a) Measured map of the ML regime as a function of I_{Gain} and V_{SA}, (b) measured autocorrelation pulse train, (c) an isolated pulse fitting by sech^2 shape, and (d) optical spectrum for $I_{Gain} = 220$ mA and $V_{SA} = -1.9$ V.

over a large SA bias range $-0.7 \leq V_{SA} \leq -1.9$ V and I_{Gain} range $104 \leq I_{Gain} \leq 220$ mA as denoted by the blue areas in Fig. 5(a). In these areas we observed optical spectra with the longitudinal modes lasing in every sixth mode at a spacing of $\sim$240 GHz [see Fig. 5(d)], and a side-mode suppression ratio (SMSR) for the intermediate (non-lasing) modes of $>$30 dB.

TABLE II
3-QW COMPARED WITH 5-QW FOR 240 GHz CPM LD

Parameters		3-QW	5-QW
Optical overlap with QWs (Γ) (%)		2.19	5
ML regime at	V	$-0.7 < V_{SA} < -1.9$	$V_{SA} = -2.0$
$M = 6$	mA	$104 \leq I_{Gain} \leq 220$	$184 \leq I_{Gain} \leq 196$
Peak power (mW)		65	28
Optical spectral width (nm)		3.95	3.49
Pulse length (ps)		0.88	1.47
TBP		0.42	0.62

As noted, the wide 240 GHz pure ML range is attributed to the higher E_{sat} characteristics of the gain media and the fast absorption recovery times in AlGaInAs QWs, which has been measured to be $<$5 ps for an applied reverse bias above 3 V [29]. The ratio of E_{sat} between the gain and absorber media determines the range of stable ML [40]. The SA absorption recovery time determines the highest pure ML frequency achievable, and a recovery time $<$5 ps is sufficient for producing pure 240 GHz pedestal-free ML pulses [41].

As anticipated, the equivalent laser fabricated using a 5-QW Al-quaternary structure [14] with a Γ value of 5% resulted in a less broad range for stable harmonic ML and a lower average output power. Pure ML with $\sim$100% modulation at $\sim$240 GHz was obtained with $V_{SA} = -2.0$ V, 184 mA $\leq I_{Gain} \leq$ 196 mA. Table II summarizes a comparison of the 240 GHz CPM LD based on the 3-QW and 5-QW structures.

Although CPM is an excellent approach for reaching modest harmonic numbers, because of the finite length of the SA, it is difficult in practice to design CPM lasers to mode-lock at harmonics higher than $\sim$10.

V. COUPLED-CAVITY MODE LOCKING (CCM)

In coupled cavity ML (CCM), a short cavity is created within the laser and is coupled into a longer cavity such that the ratio of the cavity lengths is an integer. The shorter cavity determines the mode-locking frequency while the longer cavity provides the gain required for stable operation and contains the SA. The theoretical analysis performed in [11] implied that, while the accurate positioning of intra-cavity reflectors (ICRs) in the cavity was important for CCM operation, the stability of the CCM regime could be potentially higher than that of the rival CPM approach due to the strong linear modal selectivity of the compound cavity. We have used the CCM approach to transfer the idea presented in [11] to the telecoms-relevant wavelength of 1.5 μm [42] in which we focused primarily on the device performance of ridge waveguide lasers with a single- and 2- slot ICR.

The device is based on 5-QWs and its layout is shown in Fig. 6. The currents applied to gain Sections I and II are I_{GS1} and I_{GS2} respectively. According to simulations [12], lasers with a single- and 2-slot ICRs should have the best ML operation at the harmonic number $M = 4$.

Fig. 7 shows the measured autocorrelation traces and their corresponding optical spectra for single- and 2-slot ICR lasers.

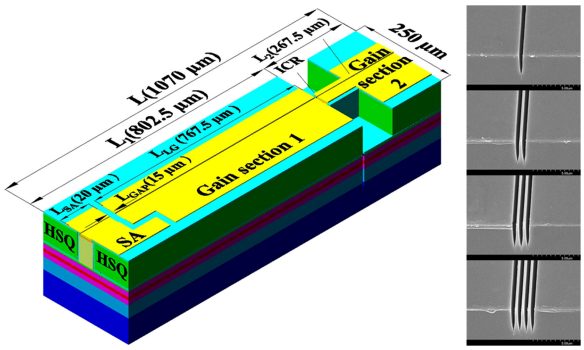

Fig. 6. Schematic of monolithic compound cavity mode-locked laser with single-slot ICR; scanning electron microscope (SEM) cross-section pictures of a cleaved laser wafer with single- and multi-slots mirrors etched to a depth of ~3.2 μm. The length of the laser is L, and the lengths of gain Sections 1 and 2 are L_1 and L_2 respectively

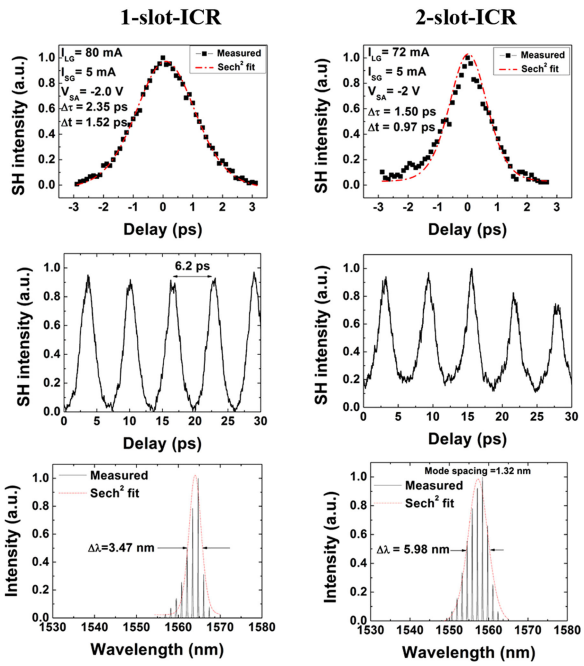

Fig. 7. Measured autocorrelation traces and the corresponding optical spectra of the lasers with 1- and 2-slot-ICRs, respectively.

It is apparent that, at the harmonic number $M = 4$, the laser with a single-slot ICR produced the best ML operation which again is in good agreement with the simulated results in [12], [42]. Pure HML of the device at harmonic number of $M = 4$ was observed by forward biasing the two gain sections ($60\,\text{mA} \leq I_{GS1} \leq 80\,\text{mA}$, $0\,\text{mA} \leq I_{GS2} \leq 20\,\text{mA}$) and reverse biasing the absorber section ($|V_{SA}| \geq 2.0\,\text{V}$). Under the experimental conditions of $V_{SA} = -2.0\,\text{V}$, $I_{GS1} = 80\,\text{mA}$, $I_{GS2} = 5\,\text{mA}$, the pulse autocorrelation trace had a width of 2.35 ps, which deconvolves to a 1.52 ps pulse duration, assuming a sech^2 pulse shape. The pulse repetition frequency was 161.8 GHz, which is in accordance with the mode spacing in the optical spectrum. The wavelength was centered at 1564 nm with a 3 dB bandwidth of 3.47 nm. The time-bandwidth product (TBP) of the pulse is equal to 0.65, which is somewhat larger than the transform-limited value (≈ 0.315) of a pulse with a sech^2 profile. This is believed to be due to SPM in the gain section [32].

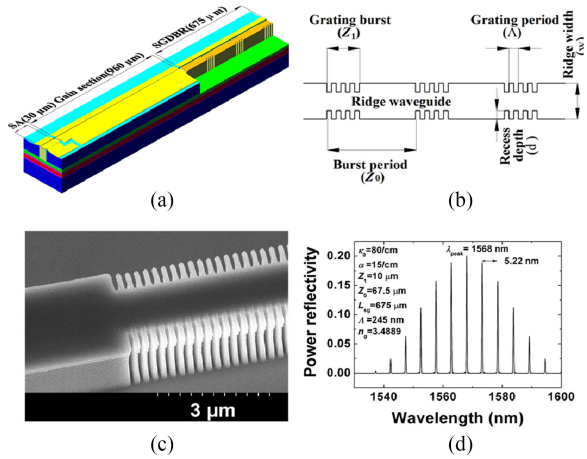

Fig. 8. (a) Schematic of the entire device, (b) configuration of the SGDBR, (c) SEM picture of the first-order sidewall gratings with a 0.6 μm recess, (d) simulation of sample grating power reflectivity plotted against wavelength.

For the 2-slot-ICR case, HML was observed with a slight Q-switching envelope at $M = 4$ over the following bias ranges: forward biasing the two gain sections ($40\,\text{mA} \leq I_{GS1} \leq 72\,\text{mA}$, $0\,\text{mA} \leq I_{GS2} \leq 10\,\text{mA}$) and reverse biasing the absorber section ($|V_{SA}| \geq 2.0\,\text{V}$). The shortest pulse width of 0.97 ps was observed with $V_{SA} = -2.0\,\text{V}$, $I_{GS1} = 72\,\text{mA}$, $I_{GS2} = 5\,\text{mA}$, and the corresponding TBP is 0.72.

CCM devices can be difficult to manufacture as the fabrication process generally depends critically on cleaving to precision tolerances. At low values of M, cleaving is straightforward, but at $M > 15$, small errors in cleaving (~0.5%) can result in the incorrect value of M being selected [12]. Although we have demonstrated ML operation at up to 2.1 THz in the GaAs material system [11], for the lower gain quaternary systems at 1.5 μm, ML operation much above 240 GHz has been very poor.

VI. Sampled Grating DBR Mode-Locking (SGDM)

In order to overcome the disadvantages of CPM and CCM lasers, we have recently proposed the use of SGDBR structures for reaching THz repetition frequencies. The SGDBR provides strong frequency selectivity at the mode-locked frequency while the 'soft walls' of the reflectors relax fabrication tolerances and ensure the long cavity can self-adjust to supporting an integral number of mode-locked periods [43].

The fabricated device structure along with its dimensions is shown in Fig. 8(a). Fig. 8(b) shows the SGDBR configuration schematically. The burst period of the grating (Z_0) which determines the mode-locked frequency is 67.5 μm, and the length of a grating burst (Z_1) is 10 μm. The number of sample periods N_s is 10, and the SGDBR length (L_{SG}) amounts to $N_s \times Z_0$. The grating burst is of first-order with a 50% duty cycle and formed by etching recesses of depth $d = 0.6$ μm into the sidewalls of the waveguide, as shown in Fig. 8(c). The grating period (Λ) is 245 nm for a 1.56 μm Bragg wavelength, which is intention-

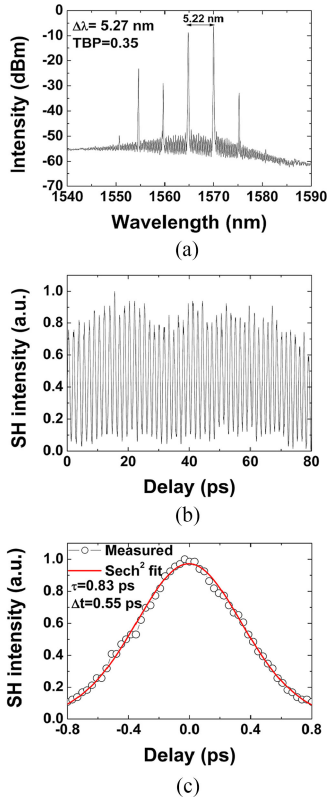

Fig. 9. The device performance under the operation conditions of $V_{SA} = -3\,\mathrm{V}$, $I_{SG} = 0\,\mathrm{mA}$: (a) optical spectrum at the point of $I_{Gain} = 192\,\mathrm{mA}$, (b) corresponding autocorrelation traces showing ML F_r of 637 GHz, and (c) an isolated AC pulse fitted in red by a sech^2 pulse shape.

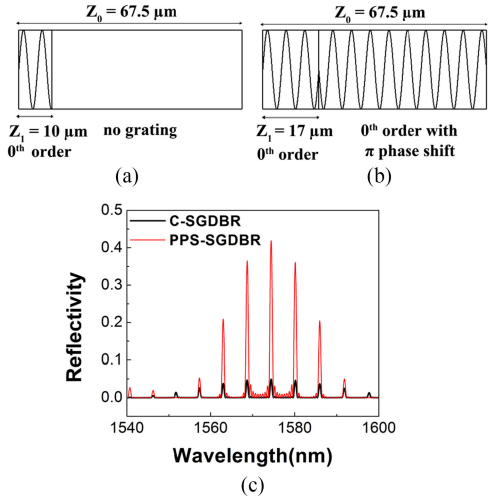

Fig. 10. Device structures based on (a) C-SGDBR, (b) PPS-SGDBR, and (c) simulated reflection spectra for C-SGDBR and PPS-SGDBR.

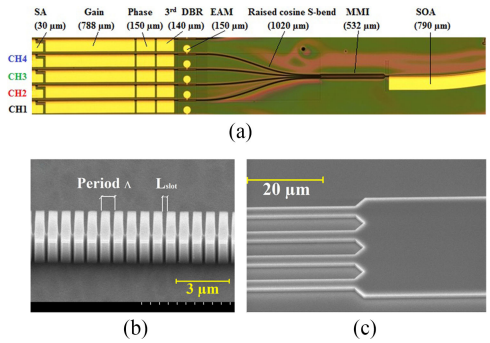

Fig. 11. (a) Optical microscope picture of the overall 40 GHz DBR mode locked laser array, (b) SEM picture of a cross section of the ridge waveguide, (c) surface-etched third-order gratings, (d) input to MMI coupler section.

ally red-shifted from the photoluminescence wavelength of the 5-QW active layer at 1.53 μm in order to reduce the absorption loss in the SGDBR section. The coupling coefficient of an unsampled grating, κ_0, was measured to be approximately 80 cm^{-1} using the sub-threshold spectral fitting method [44]. F_r was designed to be 0.64 THz, and corresponds to $c/(2n_g Z_0)$, where c is the velocity of light in free space, and n_g is the group index. Thus, F_r is inversely proportional to Z_0, and the maximum possible F_r is limited by the optical gain-bandwidth of the device. The calculated power reflection spectrum of the SGDBR grating, taking account of the linear propagation loss with the DBR section unbiased, is shown in Fig. 8(d), in which the central peak wavelength (λ_{peak}) is 1568 nm and the spacing between reflectivity peaks is about 5.22 nm, and corresponds to $(\lambda_{peak})^2/(2n_g Z_0)$.

Pure ML operation at around 640 GHz with nearly transform limited pulse characteristics was observed for a large range of laser parameters: I_{Gain} varied from 60 mA to 250 mA, V_{SA} from 0 V to -3.0 V, and I_{DBR} varied from 0 mA to 20 mA (below the I_{th} of the SGDBR section).

The optical spectrum with $I_{Gain} = 192\,\mathrm{mA}$ is shown in Fig. 9(a). The central wavelength is 1567.89 nm with a channel spacing of 5.22 nm and a 3 dB bandwidth of 5.27 nm. The spacing of the peak wavelength between adjacent channels is consistent with the simulation results in Fig. 8(d) and corresponds to an F_r of $\sim$637 GHz. The measured AC trace is shown in Fig. 9(b), under the following bias conditions: $V_{SA} = -3.0\,\mathrm{V}$, $I_{Gain} = 192\,\mathrm{mA}$, and $I_{SG} = 0\,\mathrm{mA}$. The average period of the measured emitted pulse train was 1.57 ps, which also corresponds to an F_r of 637 GHz, in accordance with the optical spectrum mode spacing shown in Fig. 9(a). The AC width of an isolated pulse was 0.83 ps, which deconvolves to a pulse width of 0.55 ps, assuming a sech^2 pulse shape [see Fig. 9(c)]. The time-bandwidth product (TBP) of the pulse is equal to 0.35, which is nearly at the transform-limit (≈ 0.315) for a sech^2 pulse shape.

When operated with a smaller reverse voltage applied to the SA, such as $V_{SA} = -2.3$ V, and a higher gain section current ($I_{Gain} \geq 295\,\mathrm{mA}$), operation at the second harmonic, with $F_r = 1.28\,\mathrm{THz}$, was also achieved [43].

In order to increase the effective coupling coefficient, κ, of the SGDBR, we have recently developed specially designed sampled gratings with phase shifted sections [15]. Fig. 10 illustrates a C-SGDBR and a π-phase shifted SGDBR (PPS-SGDBR). When the duty cycle of the PPS-SGDBR is chosen to be $Z_1/Z_0 = 0.25$, the different order peaks in the reflection spectrum are most uniform. The effective κ of the PPS-SBG is expected to be more than three times $((67.5 - 2 \times 17)/10 = 3.35)$ that of a C-SGDBR and

nearly 1/2 ($((67.5 - 2 \times 17)/67.5 = 0.4963$) that of a uniform grating. Transfer matrix simulations of the reflectivity of the two kinds of SGDBR, calculated confirm this analysis [see Fig. 10(c)]. In this fabrication run, $\kappa \approx 23.2\,\mathrm{cm}^{-1}$ for the 0^{th}-order uniform grating, lower than the expected value of $80\ \mathrm{cm}^{-1}$ because of the reactive ion etch (RIE) lag effect. The measured results of the fabricated PPS-SGDBR MLLs confirmed that the use of a PPS-SGDBR did increase the effective coupling coefficient as we simulated [15].

Compared with the CCM and CPM techniques that require complicated fabrication steps and high precision cleaving, MLLDs based on SGDBRs have several advantages. The SGDBR accurately determines the wavelength of operation and acts as a filter, providing strong selection of only the modes desired for ML, while the spatial tolerance for the length of the main cavity is relaxed by the 'soft-walled' gratings. At the same time, pulses are reflected into the main cavity from along the distributed length of the grating; provided the grating is sufficiently long the laser is able to self adjust so that the spectral resonances of the SGDBR align with a sub-set of the resonant frequencies of the main cavity. The SGDBR concept relaxes the stringent fabrication and cleaving tolerances associated with other HML constructions (CPM and CCM), so devices can be fabricated as readily as conventional ridge waveguide lasers. This class of device therefore represents a significant advancement in the HML field.

VII. Monolithic Multi-Color Mode-Locked Laser Array

As described in Section II, MLLDs can be monolithically integrated with other components. Here we demonstrate a multi-wavelength mode-locked laser array. Such devices are ideal candidates for high-speed optical sampling, photonic microwave systems and next generation optical communication systems [45], [46]. Compared to their hybrid integrated module counterparts containing several discrete devices, monolithically integrated mode-locked DBR laser diode (MLDLD) arrays can reduce system costs by simplifying optical alignment and packaging processes. By eliminating multiple coupling losses into fibers, the energy efficiency is also improved. Here, we use our simple, flexible approach of surface etched gratings and QWI to integrate monolithically four 40 GHz 1.55 μm AlGaInAs/InP mode-locked DBR lasers, four electroabsorption modulators, a 4×1 multi-mode interference (MMI) coupler, and a semiconductor optical amplifier (SOA) [47]. The design of the DBR sections was optimized with third-order surface-etched Bragg gratings, a moderate coupling efficiency ($\kappa \sim 65\ \mathrm{cm}^{-1}$), and low absorption and scattering losses [21]. The period Λ of the DBR varied from 734 to 740 nm for channel (CH) 1 to CH4 respectively. The 5-QW structure was used, and an optical microscope picture and the dimensions of the device are shown in Fig. 11.

Fig. 12 shows the ML maps as a function of the gain current (I_{Gain}) and reverse voltage applied to the SA (V_{SA}) for the four channels. 40 GHz pure ML (PML) characteristics were observed for I_{Gain} between 120 mA and 300 mA and for $|V_{SA}| \geq 2.0\,\mathrm{V}$. We found the pulse widened when the value of I_{Gain} was increased and shortened when the value of $|V_{SA}|$ was increased, with the shortest pulse width lying between 2.63 and 2.85 ps. Adjacent to PML area, regions of ML with self-pulsation (SP) were observed. With $|V_{SA}| < 2.0\,\mathrm{V}$, incomplete ML (IML), i.e. less than 100% modulation, was observed.

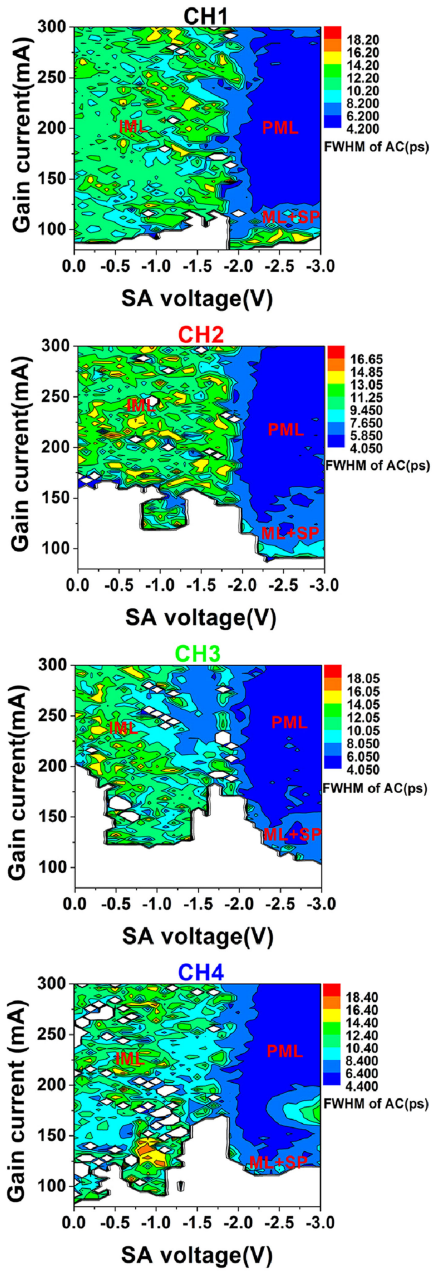

Fig. 12. Mode locking map for the four channels with the EAMs floating and SOA current set to 100 mA.

Fig. 13 shows the measured optical spectra and corresponding autocorrelation traces at an operating point at the right-top corner of Fig. 12. The peak wavelengths in nm from CH1 to CH4 are 1560.77 (designed wavelength 1560.00), 1564.02 (1564.25), 1567.86 (1568.50), 1572.76 (1572.75), respectively. The FWHM of the optical spectra of the four channels are 1.07, 1.51, 1.67, 1.36 nm and the corresponding deconvolved FWHM of the pulse widths are 4.28, 3.58, 3.19, and 3.5 ps assuming a sech^2 pulse shape. The corresponding time-bandwidth prod-

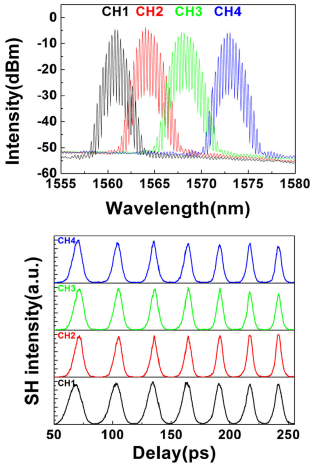

Fig. 13. Measured optical spectra (top) and autocorrelation traces (bottom) of the four channels when $V_{SA} = -3$V, $I_{Gain} = 300$ mA, $I_{SOA} = 100$ mA and other sections are floating.

ucts (TBPs) are 0.56, 0.66, 0.65, and 0.58. The measured RF frequencies were 38.01, 38.43, 38.57, and 38.43 GHz.

Fig. 14 shows pulse repetition frequency (F_r) tuning using the DBR injection current for the four channels. We note typical trends, i.e. for all investigated V_{SA} and for a fixed I_{Gain}, F_r decreases with increasing I_{DBR}. The frequency reduction with increasing I_{DBR} was consistent with the increase in the effective length due to lower absorption loss [48]. On the other hand, for a fixed value of I_{DBR} and V_{SA}, F_r decreased with increasing I_{Gain}. These anomalously high frequency shifts are mainly caused by the detuning of the cavity roundtrip frequency by gain/absorber saturation effects [49].

Here we note that the SA section can also be used to synchronize the ML frequency to an electrical RF input (hybrid ML). We can use the DBR to tune the peak wavelength and ML frequency, and use the EAM for encoding at >10 Gb/s in each channel. The four channels can be operated either individually or simultaneously, and, using either electrical or optical injection, can be easily synchronized to operate at the same F_r of 40 GHz with designated wavelength registration for optical code division multiple access (OCDMA) or optical time division multiple access (OTDMA) systems applications [22].

VIII. Conclusion

We have reviewed the design evolution of MMLDs as the ML frequency increases from 40 GHz to >1 THz. At frequencies below ~50 GHz, ML at the fundamental round trip frequency is practical, but the low gain in materials for 1.5 μm operation mandate HML operation for higher frequencies. The difficulties of precision cleaving of short cavities, coupled with a desire for higher power, make long cavity lengths desirable. It then becomes necessary to control the SPM effect in long cavity length devices by reducing the cavity losses and increasing the saturation energy (E_{sat}), which in turn can be achieved by reducing number of QWs. We have designed a novel epitaxial laser wafer structure with a 3-QW active layer integrated with a passive FRL. AlGaInAs/InP MLLs operating at 40 GHz have a significantly improved internal loss, slope efficiency, ML

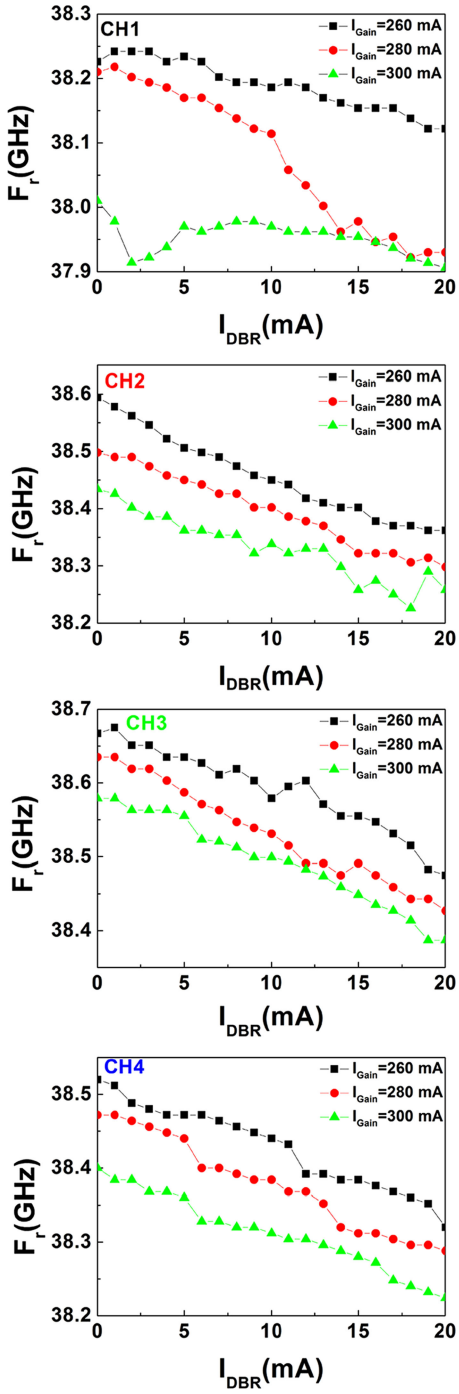

Fig. 14. Pulse repetition frequency tuning using IDBR with the $V_{SA} = -3$V, EAMs floating and SOA current set to 100 mA for the four channels.

range, RF linewidth, timing jitter, and FFP. Pulse lengths of 0.7 to 1 ps were obtained from all-active MLLDs. This was further reduced by making part of the cavity a transparent passive waveguide using QWI: without any external pulse compression, nearly transform-limited Lorentzian pulses were generated at a ~38 GHz repetition frequency with a pulse duration of 490 fs, the shortest pulse duration from any electrically pumped QW MLLD.

We also have discussed the evolution of HML concepts of increasing sophistication, starting from a simple construction with ML operation at the fundamental cavity round trip frequency of 40 GHz to a number of HML designs operating at up to 1.28 THz. All of the devices were fabricated using simple flexible and low-cost techniques – side-wall or surface-etched gratings and QWI. In order to increase the ML frequency, we demonstrated HML using CPM (240 GHz), CCM (160 GHz), and SGDM constructions (640 GHz and 1.28 THz). Compared to the CPM and CCM methods, SGDM devices relax stringent fabrication and cleaving tolerances, and stable HML is observed over a wide range of bias parameters in terms of drive currents and bias to the gain and SA sections. Finally, we reported a monolithic multi-color mode-locked laser array fabricated in the AlGaInAs/InP material system. The four channels can be operated either individually or simultaneously, and, using either electrical or optical injection, can be synchronized to operate at the same F_r of 40 GHz, with designated wavelength registration suitable for optical code division multiple access (OCDMA) or optical time division multiple access (OTDMA) systems applications.

ACKNOWLEDGMENT

The authors would like to acknowledge the staff of the James Watt Nanofabrication Centre at the University of Glasgow for help in fabricating the devices.

REFERENCES

[1] J Y. K. Chen, M. C. Wu, T. Tanbun-Ek, R. A. Rogan, and M. A. Chin, "Subpicosecond monolithic colliding pulse mode-locked multiple quantum well lasers," *Appl. Phys. Lett.*, vol. 58, pp. 1253–1255, 1991.

[2] K. Yvind *et al.*, "Low-jitter and high- power 40-GHz all-active mode-locked lasers," *IEEE Photon. Technol. Lett.*, vol. 16, no. 4, pp. 975–977, Apr. 2004.

[3] Y.-C. Xin *et al.*, "Monolithic 1.55 μm GaInNAsSb quantum well passively modelocked lasers," *Electron. Lett.*, vol. 44, no. 9, pp. 581–582, 2008.

[4] E. L. Portnoi and A. V. Chelnokov, "Passive mode-locking in a short cavity laser," in *Proc. Dig. 12th IEEE Semiconductor Conf.*, Davos, Switzerland, 1990, pp. 140–141.

[5] Y. Wen, D. Novak, H. Liu, and A. Nirmalathus, "Generation of 140 GHz optical pulses with suppressed amplitude modulation by subharmonic synchronous mode locking of Fabry-Perot semiconductor laser," *Electron. Lett.*, vol. 37, no. 9, pp. 581–582, 2001.

[6] Y. K. Chen, M. C. Wu, T. Tanbun-Ek, R. A. Logan, and M. A. Chin, "Subpicosecond monolithic colliding-pulse mode-locked multiple quantum well lasers," *Appl. Phys. Lett.*, vol. 58, pp. 1253–1255, 1991.

[7] J. F. Martins-Filho, E. A. Avrutin, C. N. Ironside, and J. S. Roberts, "Monolithic multiple colliding pulse mode-locked quantum-well lasers: Experiment and theory," *IEEE J. Sel. Topics Quantum Electron.*, vol. 1, no. 2, pp. 539–551, Jun. 1995.

[8] Y. Katagiri and A. Takada, "A harmonic colliding-pulse mode-locked semiconductor laser for stable subterahertz pulse generation," *IEEE Photon. Technol. Lett.*, vol. 9, no. 11, pp. 1442–1444, Nov. 1997.

[9] T. Shimizu, I. Ogura, and H. Yokoyama, "860 GHz rate asymmetric colliding pulse mode locked diode lasers," *Electron. Lett.*, vol. 33, no. 22, pp. 1868–1869, 1997.

[10] S. Arahira, Y. Matsui, and Y. Ogawa, "Mode-locking at very high repetition rates more than terahertz in passively mode-locked distributed-Bragg-reflector laser diodes," *IEEE J. Quantum Electron.*, vol. 32, no. 7, pp. 1211–1224, Jul. 1996.

[11] D. A. Yanson *et al.*, "Ultrafast harmonic mode-locking of monolithic compound-cavity laser diodes incorporating photonic-bandgap reflectors," *IEEE J. Quantum Electron.*, vol. 38, no. 1, pp. 1–11, Jan. 2002.

[12] L. Hou *et al.*, "160 GHz passively mode-locked AlGaInAs 1.55 μm strained quantum-well lasers with deeply etched intracavity mirrors," *IEEE J. Sel. Topics Quantum Electron.*, vol. 19, no. 4, Jul./Aug. 2013, Art. No. 1100409.

[13] L. Hou, M. Haji, and J. H. Marsh, "Mode locking at terahertz frequencies using a distributed Bragg reflector laser with a sampled grating," *Opt. Lett.*, vol. 38, pp. 1113–1115, 2013.

[14] L. Hou, M. Haji, and J. H. Marsh, "Mode-locking and frequency mixing at THz pulse repetition rates in a sampled-grating DBR mode-locked laser," *Opt. Exp.*, vol. 22, pp. 21690–21700, 2014.

[15] L. Hou, S. Tang, and J. H. Marsh, "THz repetition frequency mode-locked laser using novel sampled gratings," to be presented at CLEO/Europe, 2017.

[16] L. Hou *et al.*, "Subpicosecond pulse generation at quasi-40-GHz using a passively mode locked AlGaInAs/InP 1.55 μm strained quantum well laser," *IEEE Photon. Technol. Lett.*, vol. 21, no. 23, pp. 1731–1733, Dec. 1, 2009.

[17] O. Kowalski *et al.*, "A universal damage induced technique for quantum well intermixing," *Appl. Phys. Lett.*, vol. 72, pp. 581–583, 1998.

[18] L. Hou, M. Haji, R. Dylewicz, B. Qiu, and A. C. Bryce, "Monolithic 45-GHz mode-locked surface-etched DBR laser using quantum-well intermixing technology," *IEEE Photon. Technol. Lett.*, vol. 22, no. 14, pp. 1039–1041, Jul. 15, 2010.

[19] S. Gee, G. Alphonse, J. Connolly, and P. J. Delfyett, "High-power mode-locked external cavity semiconductor laser using inverse bow-tie semiconductor optical amplifiers," *IEEE J. Sel. Topics Quantum Electron.*, vol. 4, no. 2, pp. 209–215, Mar./Apr. 1998.

[20] L. Hou, M. Haji, and J. H. Marsh, "Monolithic mode-locked laser with an integrated optical amplifier for low-noise and high-power operation," *IEEE J. Sel. Topics Quantum Electron.*, vol. 19, no. 4, Jul./Aug. 2013, Art. No. 1100808.

[21] L. Hou *et al.*, "Monolithic 40-GHz passively mode-locked AlGaInAs–InP 1.55-μm m MQW laser with surface-etched distributed bragg reflector," *IEEE Photon. Technol. Lett.*, vol. 22, no. 20, pp. 1503–1505, Oct. 15, 2010.

[22] L. Hou, M. Haji, B. Qiu, and A. C. Bryce, "Mode-locked laser array monolithically integrated with MMI combiner, SOA, and EA modulator," *IEEE Photon. Technol. Lett.*, vol. 23, no. 15, pp. 1064–1066, Aug. 1, 2011.

[23] L. Hou, M. Haji, J. Akbar, B. Qiu, and A. C. Bryce, "Low divergence angle and low jitter 40 GHz AlGaInAs/InP 1.55 μm mode-locked lasers," *Opt. Lett.*, vol. 36, pp. 966–968, 2011.

[24] I. B. Petrescu-Prahova *et al.*, "High d/gamma values in diode laser structures for very high power," *Proc. SPIE , High-Power Diode Laser Technology and Applications VII*, vol. 7198, 2009, Art. No. 719811.

[25] K. Merghem, "Short pulse generation using a passively mode locked single InGaAsP/InP quantum well laser," *Opt. Exp.*, vol. 16, pp. 10675–10683, 2008.

[26] C. H. Henry, "Phase noise in semiconductor lasers," *J. Lightw. Technol.*, vol. JLT-4, no. 3, pp. 298–311, Mar. 1986.

[27] A. Shen *et al.*, "Active mode-locking of quantum dot Fabry-Perot laser diode," in *Proc. IEEE 20th Int. Semicond. Laser Conf.*, 2006, pp. 153–154.

[28] B. Qiu, S. D. McDougall, X. Liu, G. Bacchin, and J. H. Marsh, "Design and fabrication of low beam divergence and high kink-free power lasers," *IEEE J. Quantum Electron.*, vol. 41, no. 9, pp. 1124–1130, Sep. 2005.

[29] R. P. Green *et al.*, "Fast saturable absorption and 10 GHz wavelength conversion in Al-quaternary multiple quantum wells," *Opt. Exp.*, vol. 19, pp. 9737–9743, 2011.

[30] E. Avrutin, V. Nikolaev, and D. Gallagher, "Monolithic mode-locked semiconductor lasers," in *Optoelectronic Devices*. New York, NY, USA: Springer, 2005, pp. 185–215.

[31] L. A. Coldren, S. W. Corzine, and M. L. Mashanovitch, *Diode Lasers and Photonic Integrated Circuits*, vol. 218. New York, NY, USA: Wiley, 2012.

[32] G. P. Agrawal and N. A. Olsson, "Self-phase modulation and spectral broadening of optical pulses in semiconductor laser amplifier," *IEEE J. Quantum Electron.*, vol. 25, no. 11, pp. 2297–2306, Nov. 1989.

[33] M. J. R. Heck *et al.*, "Passively mode-locked 4.6 and 10.5 GHz quantum dot laser diodes around 1.55 μm with large operating regime," *IEEE J. Sel. Topics Quantum Electron.*, vol. 15, no. 3, pp. 634–643, May/Jun. 2009.
[34] M. J.R. Heck *et al.*, "Observation of Q-switching and mode-locking in two-section InAs/InP (100) quantum dot lasers around 1.55 μm," *Opt. Exp.*, vol. 15, no. 25, pp. 16292–16301, 2007.
[35] Z. Lu *et al.*, "An L-band monolithic InAs/InP quantum dot mode-locked laser with femtosecond pulses," *Opt. Exp.*, vol. 17, pp. 13609–13614, 2009.
[36] K. Merghem *et al.*, "Pulse generation at 346 GHz using a passively mode locked quantum-dash-based laser at 1.55 μm," *Appl. Phys. Lett.*, vol. 94,2009, Art. No. 021107.
[37] D. J. Derickson *et al.*, "Short pulse generation using multisegment mode-locked semiconductor lasers," *IEEE J. Quantum Electron.*, vol. 28, no. 10, pp. 2186–2202, Oct. 1992.
[38] L. Hou, M. Haji, J. H. Marsh, and A. C. Bryce, "490 fs pulse generation from a passive C-band AlGaInAs/InP quantum well mode-locked laser," *Opt. Lett.*, vol. 37, pp. 773–775, 2012.
[39] L. Hou, M. Haji, and J. H. Marsh, "240 GHz pedestal-free colliding-pulse mode-locked laser with a wide operation range," *Laser Phys. Lett.*, vol. 11, 2014, Art. No. 115804.
[40] H. Haus, "Theory of mode locking with a slow saturable absorber," *IEEE J. Quantum Electron.*, vol. QE-11, no. 9, pp. 736–746, Sep. 1975.
[41] J. Karin *et al.*, "Ultrafast dynamics in field-enhanced saturable absorbers," *Appl. Phys. Lett.*, vol. 64, pp. 676–678, 1994.
[42] L. P. Hou *et al.*, "160-GHz harmonic mode-locked AlGaInAs 1.55 μm strained quantum well compound cavity laser," *Opt. Lett.*, vol. 35, no. 23, pp. 3991–3993, 2010.
[43] L. Hou, M. Haji, and J. H. Marsh, "Mode locking at terahertz frequencies using a distributed Bragg reflector laser with a sampled grating," *Opt. Lett.*, vol. 38, pp. 1113–1115, 2013.
[44] T. Nakura and Y. Nakano, "LAPAREX-An automatic parameter extraction program for gain-and index-coupled distributed feedback semiconductor lasers, and its application to observation of changing coupling coefficients with currents," *IEICE Trans. Electron.*, vol. 83, pp. 488–495, 2000.
[45] J. Lou, T. Carruthers, and M. Currie, "4 $\times$ 10 GHz mode-locked multiple-wavelength fiber laser," *IEEE Photon. Technol. Lett.*, vol. 16, no. 1, pp. 51–53, Jan. 2004.
[46] M. M. Mielke, G. A. Alphonse, and P. J. Delfyett, "Multiwavelength mode-locked semiconductor lasers for photonic access network applications," *IEEE J. Sel. Areas Commun.*, vol. 25, no. 3, pp. 120–128, Apr. 2007.
[47] L. Hou, I. Eddie, and J. H. Marsh, "Monolithic multi-colour 40 GHz mode-locked laser array," in *Proc. Conf. Lasers Electro-Opt.*, 2016, pp. 1–2.
[48] I. Ogura, H. Kurita, T. Sasaki, and H. Yokoyama, "Precise operation-frequency control of monolithic mode-locked laser diodes for high-speed optical communication and all-optical signal processing," *Opt. Quantum Electron.*, vol. 33, pp. 709–725, 2001.
[49] S. Arahira and Y. Ogawa, "Repetition–frequency tuning of monolithic passively mode-locked semiconductor lasers with integrated extended cavities," *IEEE J. Quantum Electron.*, vol. 33, no. 2, pp. 255–264, Feb. 1997.

John H. Marsh (M'91–SM'91–F'00) received the graduate degree (B.A.) from the Universities of Cambridge, Liverpool (M.Eng.) and Sheffield (Ph.D.). He is currently a Professor of optoelectronic systems at the University of Glasgow, Glasgow, U.K., and is currently the Dean of the University of Glasgow UESTC, Chengdu Shi, China. His experience of semiconductor laser technology and integrated optics ranges from epitaxial growth through to the design and development of integrated laser modules for applications including advanced printing and imaging. His research covers fundamental electrical and optical properties of semiconductors, development of novel optoelectronic devices, processes for creating photonic integrated circuits, integrated mode-locked lasers for ultrashort pulse generation, and development and manufacturing of high-power laser array products. He co-founded Intense Ltd in 2000.

Dr. Marsh is a Fellow of the Royal Academy of Engineering, Royal Society of Edinburgh, OSA, IET, Institute of Physics and Royal Society of Arts. He received the 2006 IEEE/LEOS Engineering Achievement Award with Catrina Bryce "for extensive development and commercialization of quantum well intermixing for photonic devices." He was also received the 2006 IEEE/LEOS Distinguished Service Award "for major contributions to LEOS governance and for leadership in promoting the development of LEOS as a global society." He was thee President of the IEEE Photonics Society in 2008 and 2009.

Lianping Hou (M'11) received the B.Eng. degree from the Central-South University of Technology, Changsha, China, in 1992, the M.A. degree from Huazhong University of Science and Technology, Wuhan, China, in 2003, and the Ph.D. degree from the Chinese Academy of Sciences, Beijing, China, in 2005. In 2006, he joined the Department of Electrical and Electronic Engineering at the University of Bristol, Bristol, U.K., as a Research Associate, working on a European Commission FP6-IST Project involved with multifunctional integrated arrays of interferometer switches. In 2007, he joined the School of Engineering, University of Glasgow, Glasgow, U.K., as a Research Associate, where he worked on developing high-frequency and high-power semiconductor mode-locked lasers. In 2012, he was promoted to a Research Fellow. He is currently a Lecturer at the University of Glasgow working on nanofabrication, semiconductor laser technology, and integrated optics.

Dr. Hou is a Member of the Optical Society of America. He is the author and coauthor of more than 100 papers and the inventor of several patents.